IEEE Access
Multidisciplinary | Rapid Review | Open Access Journal

Received 6 May 2022, accepted 12 July 2022, date of publication 21 July 2022, date of current version 30 September 2022.

Digital Object Identifier 10.1109/ACCESS.2022.3193234

RESEARCH ARTICLE

A Dual-Frequency Compatible Wireless Power Transfer System With a Single Transmitter and Multiple Receivers

XIN GAO, BOCHAO DU, YUQI ZHANG, AND SHUMEI CUI
School of Electrical Engineering and Automation, Harbin Institute of Technology, Harbin 150000, China
Corresponding author: Shumei Cui (cuism@hit.edu.cn)

This work was supported in part by the National Natural Science Foundation of China under Grant 5217070714.

ABSTRACT In many applications of wireless power transfer (WPT) systems, there are situations where the transmitter needs to supply power to receivers of different frequencies or powers. Therefore, it is very important to improve its compatibility and adaptability. In this paper, a dual-frequency compatible WPT system with a single transmitter and multiple receivers is proposed. The transmitter current contains two main frequency components obtained by current modulation and resonance compensation. The receivers of different frequencies pick up the corresponding components by frequency selective resonance. Therefore, decoupled transfer and independent control can be achieved. In this paper, a dual-frequency compensation topology is constructed and an adjustment method for receiver power decoupling control is proposed. Through theoretical and experimental analysis, the efficacy characteristics of the system have been evaluated, and its dual-frequency compatibility and power decoupling control capability have been verified. Compared with the single-frequency multiple-receiver system, this system can avoid the problems of mutual coupling: induced output power and system efficiency reduction, transmitter detuning, reactive power increase and inverter output capacity reduction.

INDEX TERMS Wireless power transfer (WPT), single transmitter and multiple receivers, dual-frequency resonance, current modulation, power decoupling.

I. INTRODUCTION

Wireless power transfer (WPT) systems allow for non-contact, fully isolated power supply. It has higher reliability and greater environmental adaptability than wired power supplies. Therefore, it has received extensive attention and research [1], [2]. WPT systems have been applied in many fields such as electric vehicles, rail transportation, aerospace, mobile communication devices, home appliances, and biomedicine.

Based on the principle of minimum transmission impedance in resonant state, magnetically coupled resonant WPT systems are constructed. Different systems have different optimal operating frequencies [3]. In the case of electric vehicles, for example, the operating frequency of 85 kHz is recommended for static wireless power transfer (SWPT) systems in SAE J2954 for WPT1∼WPT3. However, there is no unified standard for dynamic wireless power transfer (DWPT) systems. Currently, experimental systems use frequencies such as 20 kHz, 40 kHz, and 85 kHz. As a result, a single transmitter may need to power receivers of different frequencies. A similar situation exists in other fields.

Therefore, it is necessary to improve the frequency and load compatibility of WPT systems with a single transmitter and multiple receivers. The specific issues are as follows.

1) Frequency compatibility: receivers with different resonant frequencies can be charged separately or simultaneously at the same transmitter. As an example, static and dynamic WPT systems for electric vehicles are shown in Fig. 1. Typical operating frequencies for DWPT and SWPT systems are f_1 (typically 20 kHz) and f_2 (typically 85 kHz), respectively [4], [5]. In systems equipped with SWPT or

The associate editor coordinating the review of this manuscript and approving it for publication was Diego Masotti.

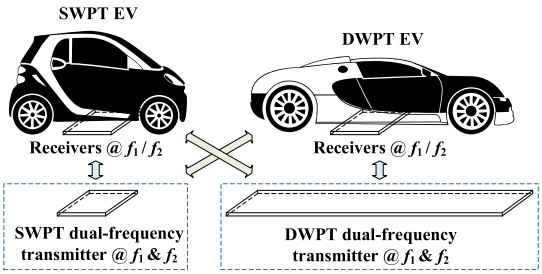

FIGURE 1. Schematic diagram of frequency compatibility.

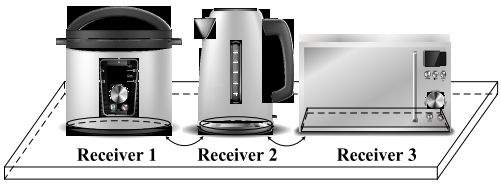

FIGURE 2. Schematic diagram of loads compatibility.

DWPT dual-frequency transmitters @ f_1& f_2, the DWPT EV @ f_1/ f_2 can also be charged at the SWPT transmitter, and similarly, the SWPT EV @ f_1 /f_2 can be charged at the DWPT transmitter. Compared with the traditional solution, receivers with two resonant frequencies are compatible in this transmitter, and they can be charged simultaneously. The energy decoupling control can be achieved through the allocation strategy. Therefore, the proposed solution can improve the compatibility and convenience of WPT systems for electric vehicles. Of course, this may require a complex system or lead to a reduction in power and efficiency, which needs to be addressed through proper design and control.

2) Load compatibility: multiple receivers can be decoupled and the output power can be adjusted independently. Take kitchen appliances as an example, as shown in Fig. 2. Due to the limited space and proximity of receivers, mutual inductance is inevitable, resulting in receiver power coupling and reducing the total output power and efficiency of the system. Therefore, decoupling and independent adjustment of the receiver output power, independent of arrangement and location, need to be achieved. This helps to reduce the size of the system and increase the power density of the system.

To solve the above problems, a dual-frequency resonant system is proposed in this paper. A single transmitter provides dual-frequency current and magnetic field, and receivers resonate in split frequencies to couple the energy.

At present, the research of multi-frequency WPT technology mainly includes wireless power transfer of multiple loads and synchronous transfer of power and information.

The research work on multi-frequency multi-load WPT systems includes both circuit topologies and control methods. In terms of control methods, [6]–[8] use the fundamental and the third harmonic of the current to transmit power together. It can avoid the output power reduction caused by mutual coupling and improve the system efficiency, but the frequency and power of the third harmonic are limited by the fundamental and the adjustment is not flexible. In terms of circuit topologies, multiple inverters coupled through a transformer are used to obtain multi-frequency primary currents to achieve separate regulation and control [9], but the power supply topology is more complex. In addition, high-order compensation topologies are used to provide multiple resonant points. It can guarantee the system resonant at each frequency point, but the independent regulation and power decoupling control needs further study. Some works use the frequency bifurcation phenomenon under the over-coupling condition and set the resonant frequencies of receivers to two bifurcated frequency points to achieve selective power transfer. But the two receivers cannot work simultaneously. Also, a hybrid modulation wave sinusoidal pulse-width modulation control method is used to generate multi-frequency hybrid currents. It simplifies the power supply topology and improves the control flexibility, but does not guarantee resonant at each frequency point.

In addition, the WPT system for simultaneous transfer of power and information is a special kind of dual-frequency system. Low-frequency and high-frequency components are used to transmit power and information separately. There are two ways to achieve this. The first method for transmitting information is to use the higher harmonic components or to inject high frequency signals [10]. However, due to the bandpass characteristics of the resonant compensation topology, the high-frequency component will be greatly attenuated. Therefore, it leads to limited information transmission frequency and communication rate. The second method is to modulate the voltage or current with the information contained in its amplitude or frequency [11]. It is effective, but the power will be significantly affected.

The above work separately verifies that a single inverter modulates multiple frequency components and multiple components are transmitted through a single coupling path. However, how to achieve simultaneous multi-frequency decoupled power transfer and independent control using a single inverter and a single transmitter remains to be investigated. It mainly involves the simultaneous resonant and decoupled control of multiple frequency components.

In this paper, a dual-frequency compatible WPT system with a single transmitter and multiple receivers is proposed. The system constructs a dual-frequency compensation topology to form two natural resonance points, which can achieve frequency compatibility of transmitters. The coupled receivers are configured with different resonant frequencies so that power decoupling can be achieved according to the frequency selective characteristics of the compensation topology. The output power of the receivers is independently controlled by a primary current modulation method to achieve load compatibility. The dual-frequency and multi-load compatibility performance of the system has been verified by theoretical analysis and experimental study.

This paper is organized as follows. Section II analyzes the principle of dual-frequency compatible WPT system

and proposes a dual-frequency compensation topology and decoupling modulation method. Section III investigates the decoupling conditions of the system, and analyzes the effects **of mutual coupling and the efficacy characteristics of the** system. A prototype is developed and experimental verification is completed in Section IV. Finally, Section V draws conclusions.

II. PROPOSED DUAL-FREQUENCY COMPATIBLE WPT SYSTEM

A. SYSTEM COMPOSITION AND PRINCIPLES

The schematic diagram of the proposed dual-frequency compatible WPT system is shown in Fig. 3. Its primary equipment consists of a high frequency inverter, a dual-frequency compensation topology and a transmitter. The system can be configured with multiple secondary devices, each of which consists of a receiver, compensation topology, high-frequency rectifier, DC/DC converter, and load. The working principle of the system is as follows.

Dual-frequency operation principle: The high frequency inverter modulates the output voltage containing two main frequency (f_1 and f_2) components, corresponding to the two resonance points of the dual-frequency compensation topology. Through the frequency selection and filtering effect of the compensation topology, a dual-frequency current flows through the transmitter and a dual-frequency alternating magnetic field is generated in space. The receivers of the corresponding resonant frequencies can receive power independently or simultaneously. Thus, frequency compatibility of the system can be achieved.

Power independent control principle: For receivers of the same frequency, the dual-frequency compensation topology is required to maintain a constant current characteristic at both resonance points in order to obtain independent induced voltages. In other words, the transmitter current is independent of the number of receivers, the degree of mutual coupling, and the output power level. Therefore, the output power of each receiver depends only on its equivalent impedance, which can be adjusted by a DC/DC converter. For receivers of different frequencies, the output power can be adjusted independently by modulating the two frequency components of the transmitter current.

Receiver decoupling principle: For two mutually coupled receivers, the resonant frequencies can be configured as f_1 and f_2 respectively. Due to the frequency selection characteristics of the compensation topology, the impedance is very high at non-resonant frequencies and essentially no current is generated. Therefore, the coupling of the receivers can be greatly reduced and the output power can be decoupled.

Based on the above principles, the proposed WPT system has dual-frequency and multi-load compatibility.

The circuit topology of the proposed system is shown in Fig. 4. The high-frequency inverter uses a single-phase full-bridge topology. The transmitter is compensated using a dual-frequency compensation topology detailed in the next section. In addition, the S topology is used to compensate the receiver. The high-frequency rectifier, DC/DC converter and load are equivalent to the load resistor. The relevant parameters and their definitions are shown in Table 1.

TABLE 1. Parameters and definitions of the system circuit topology.

Parameters	Definitions
E_d	Adjustable DC input voltage
S_1~S_4	Power electronic switches
D_1~D_4	Anti-parallel diodes
f_1, f_2	Operation frequencies
ω_1, ω_1	Operation angular frequencies
u_{iv}	Inverter output voltage
$u_{iv\_\omega_1}, u_{iv\_\omega_2}$	Two frequency components of inverter output voltage
i_{iv}	Inverter output current
$i_{iv\_\omega_1}, i_{iv\_\omega_2}$	Two frequency components of inverter output current
L_S, L_P	The transmitter's compensation inductors
C_{P1}, C_{P2}	The transmitter's compensation capacitors
L_T	Transmitter self-inductance
r_T	Transmitter resonant cavity equivalent internal resistance
i_T	Transmitter current
L_{R1}, L_{R2}	Receiver self-inductances
M_1, M_2	Mutual inductances between the transmitter and the two receivers
M_S	Mutual inductance between two receivers
C_{R1}, C_{R2}	Compensation capacitors of the receivers
r_{R1}, r_{R2}	Equivalent internal resistances of the receiver's resonant cavities
R_{R1}, R_{R2}	Equivalent load resistances of the receivers
i_{R1}, i_{R2}	Output currents of the receivers
u_{R1}, u_{R2}	Output voltages of the receivers
P_{R1}, P_{R2}	Output power of the receivers
P_R	Total output power of the receivers
η	System efficiency

B. DUAL-FREQUENCY COMPENSATION TOPOLOGY

According to the principle analysis, the compensation topology of the transmitter requires two natural resonance points, each of which maintains a constant current characteristic. The circuit diagrams of some common compensation topologies are shown in Fig. 5. Their resonant angular frequencies, output characteristics, load-independent voltages or currents, and zero impedance angle (ZPA) additional conditions are analyzed and listed in Table 2.

It can be seen that the conventional S, P, SP, and PS topologies have only one resonance point and constant voltage characteristics [12]. Moreover, the LC, LCC, CLC, and LLC topologies also have only one resonance point, despite their constant current characteristics [13]. Therefore, these topologies cannot meet the requirements of the system.

In this paper, a dual-frequency compensation topology is proposed, as shown in Fig. 6. And it is improved on the basis of the LC topology. By adding a parallel LC branch, the compensation topology is upgraded to IV order, and an additional resonance point is introduced. Its two resonant angular frequencies are represented by Equation (1), where

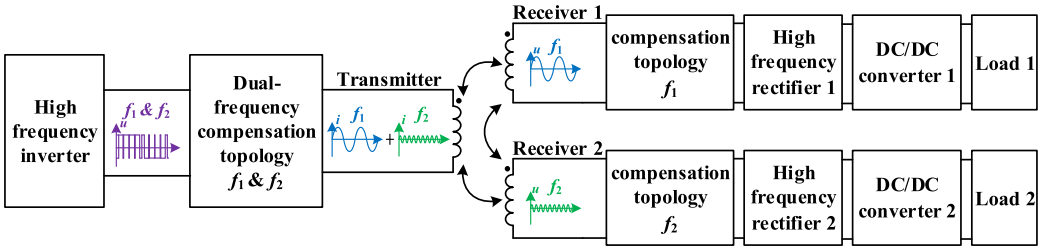

FIGURE 3. Schematic diagram of the proposed dual-frequency compatible WPT system.

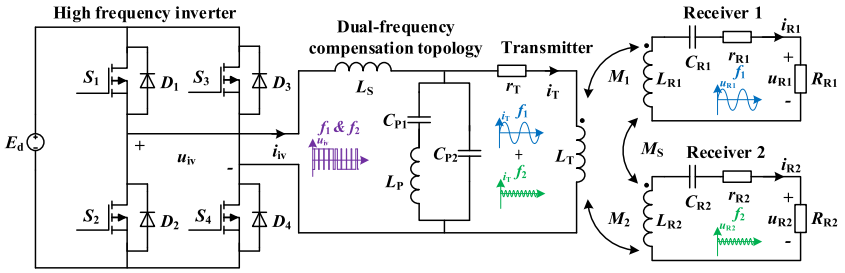

FIGURE 4. Circuit topology of the proposed WPT system.

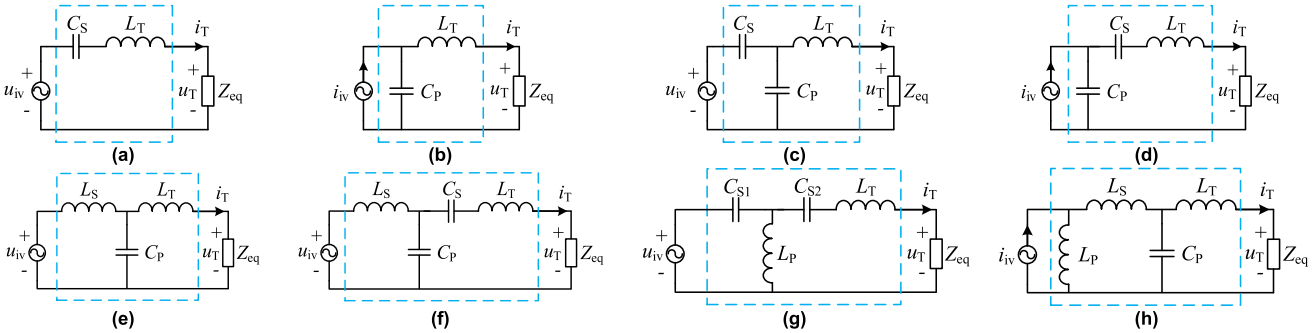

FIGURE 5. Circuit diagrams of several common compensation topologies: (a) S, (b) P, (c) SP, (d) PS, (e) LC, (f) LCC, (g) CLC and (h) LLC.

$C_{P1} = C_{P2} = C_P$.

$$\begin{cases} \omega_1 = \sqrt{(2L_S + L_P - \sqrt{L_P^2 + 4L_S^2}) \Big/ (2L_S L_P C_P)} \\ \omega_2 = \sqrt{(2L_S + L_P + \sqrt{L_P^2 + 4L_S^2}) \Big/ (2L_S L_P C_P)} \end{cases} \tag{1}$$

In addition, the topology has constant current characteristics at the two resonant frequencies mentioned above, and the corresponding load independent current components are expressed in Equation (2). The additional ZPA condition is consistent with the LC topology.

$$\begin{cases} i_{T\_\omega_1} = u_{iv\_\omega_1} / (j\omega_1 L_S) \\ i_{T\_\omega_2} = u_{iv\_\omega_2} / (j\omega_2 L_S) \end{cases} \tag{2}$$

C. DUAL-FREQUENCY DECOUPLING MODULATION METHOD

According to Equation (2), the two frequency components of the transmitter current, $i_{T\_\omega_1}$ and $i_{T\_\omega_2}$, can be independently regulated by adjusting the output voltage of the inverter. In this paper, a dual-frequency decoupling modulation method based on sinusoidal pulse width modulation (SPWM) is proposed, as shown in Fig. 7.

In Fig. 7, the angular frequencies of the modulated wave u_m and the carrier wave u_c are configured as ω_1 and ω_2, respectively, corresponding to the two resonant angular frequencies of the dual-frequency compensation topology. Their amplitudes are V_m and V_c respectively, and the modulation ratio K_A is defined as Equation (3).

$$K_A = \frac{V_m}{V_c} \tag{3}$$

The inverter output voltage then contains two main frequency components, $u_{iv\_\omega_1}$ and $u_{iv\_\omega_2}$. The result of its Fourier decomposition can be expressed as Equation (4), where J_0 is the Bessel function.

$$\begin{cases} u_{iv\_\omega 1} = K_A E_d \cos(\omega_1 t + \theta_1) \\ u_{iv\_\omega 2} = \dfrac{4E_d}{\pi} J_0\left(\dfrac{K_A \pi}{2}\right) \cos(\omega_2 t + \theta_2) \end{cases} \tag{4}$$

TABLE 2. Characteristics comparison of compensation topologies.

Orders	Compensation topologies	Circuit diagrams	Resonance angular frequencies	Output characteristics	Load-independent voltages or currents	ZPA additional conditions
I	S	Fig. 5 (a)	$\omega=\frac{1}{\sqrt{L_T C_S}}$	Constant voltage	$u_T=u_{iv}$	None
	P	Fig. 5 (b)	$\omega=\frac{1}{\sqrt{L_T C_P}}$	Constant voltage	$u_T=\frac{i_{iv}}{j\omega C_P}$	None
II	SP	Fig. 5 (c)	$\omega=\frac{1}{\sqrt{L_T(C_S+C_P)}}$	Constant voltage	$u_T=\frac{C_S u_{iv}}{C_S+C_P}$	-
	PS	Fig. 5 (d)	$\omega=\sqrt{\frac{C_S+C_P}{L_T C_S C_P}}$	Constant voltage	$u_T=\frac{i_{iv}}{j\omega C_P}$	-
	LC	Fig. 5 (e)	$\omega=\frac{1}{\sqrt{L_S C_P}}$	Constant current	$i_T=\frac{u_{iv}}{j\omega L_S}$	$L_T=L_S$
	LCC	Fig. 5 (f)	$\omega=\frac{1}{\sqrt{L_S C_P}}$	Constant current	$i_T=\frac{u_{iv}}{j\omega L_S}$	$\omega^2(L_T-L_S)C_S=1$
III	CLC	Fig. 5 (g)	$\omega=\frac{1}{\sqrt{L_P C_{S1}}}$	Constant current	$i_T=j\omega C_{S1}u_{iv}$	$\omega^2 L_T C_{S1} C_{S2}=C_{S1}-C_{S2}$
	LLC	Fig. 5 (h)	$\omega=\frac{1}{\sqrt{(L_S+L_P)C_P}}$	Constant current	$i_T=\frac{L_P i_{iv}}{L_P+L_S}$	$\omega^2 L_T L_S C_P=L_T+L_S$

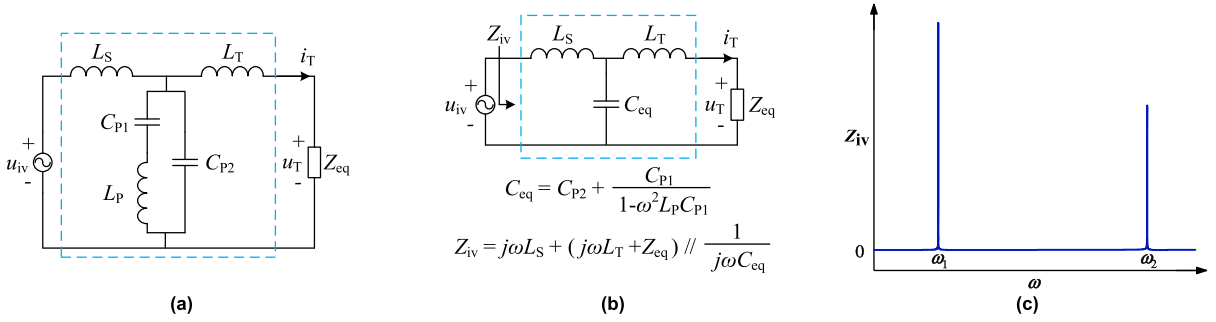

FIGURE 6. Proposed dual-frequency compensation topology: (a) circuit diagram, (b) equivalent circuit diagram and (c) spectrogram.

Substituting into Equation (2), Equation (5) can be derived.

$$\begin{cases} I_{T\_\omega_1} = \dfrac{K_A E_d}{\sqrt{2}\omega_1 L_S} \\ I_{T\_\omega_2} = \dfrac{2\sqrt{2}\,E_d}{\pi\omega_2 L_S} J_0\left(\frac{K_A\pi}{2}\right) \end{cases} \tag{5}$$

According to Equation (5), the contour lines of $i_{T\_\omega 1}$ and $i_{T\_\omega 2}$ varying with E_d and K_A are shown in Fig. 8.

In Fig. 8, for each given set of $I_{T\_\omega 1}$ and $I_{T\_\omega 2}$, there is a unique set of E_d and K_A values corresponding to it, i.e., the coordinate values where the two contour lines intersect. Take point A as an example. When transmitter currents $I_{T\_\omega 1} = 10.58$ A and $I_{T\_\omega 2} = 4.04$ A are required, $K_A = 0.62$ and $E_d = 300$ V should be set. If $I_{T\_\omega 2}$ needs to be 5.10A with a constant $I_{T\_\omega 1}$, $K_A = 0.52$ and $E_d = 360$ V can be set to point B. Similarly, if $I_{T\_\omega 1}$ needs to be 14.10A with a constant $I_{T\_\omega 2}$, $K_A = 0.72$ and $E_d = 340$ V can be set to point C.

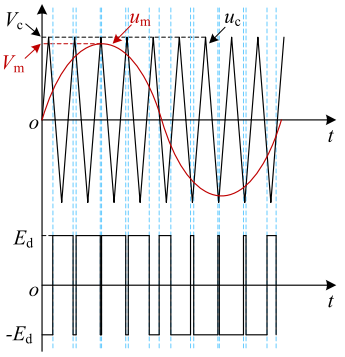

FIGURE 7. Proposed dual-frequency decoupling modulation method.

Therefore, by adjusting the DC bus voltage E_d and modulation ratio K_A, independent regulation of $I_{T\_\omega 1}$ and $I_{T\_\omega 2}$ can be achieved. Therefore, the dual-frequency decoupling

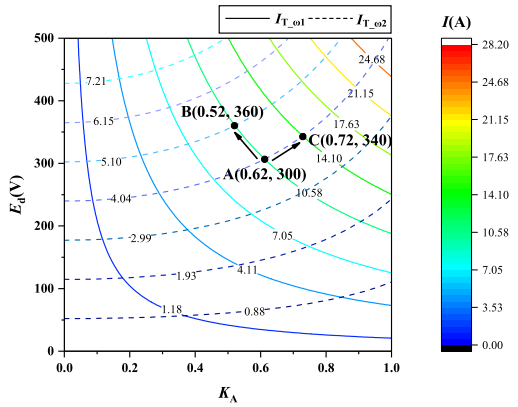

FIGURE 8. Contour lines of $I_{T\_\omega1}$ and $I_{T\_\omega2}$ varying with E_d and K_A.

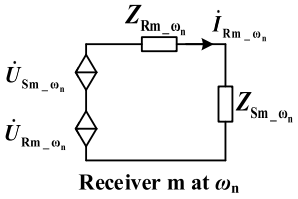

FIGURE 9. Equivalent circuit of the receiver.

modulation are realized. Since the compensation topology has constant current characteristics, there are various feasible methods in practical applications, such as off-line calculation, table look-up method, closed-loop control, etc.

D. EQUIVALENT MODEL OF THE RECEIVER

The equivalent circuit of receiver m (m = 1, 2) at the angular frequency ω_n (n = 1, 2) is shown in Fig. 9. The definitions and expressions of each parameter are shown in Table 3.

E. DECOUPLING CONDITIONS AND INFLUENCING FACTORS

Based on the equivalent circuit in Fig. 9, the receiver current is derived as Equation (6). As a comparison, the fully decoupled current should be expressed as Equation (7).

$$\begin{aligned}\dot{I}_{R1} &= \dot{I}_{R1\_\omega_1} + \dot{I}_{R1\_\omega_2} \\ &= \frac{\dot{U}_{R1\_\omega_1} + \dot{U}_{S1\_\omega_1}}{Z_{R1\_\omega_1} + Z_{S1\_\omega_1} + \frac{\dot{U}_{R1\_\omega_2} + \dot{U}_{S1\_\omega_2}}{Z_{R1\_\omega_2} + Z_{S1\_\omega_2}}}\end{aligned} \tag{6}$$

$$\dot{I}_{R1} = \dot{I}_{R1\_\omega_1} = \frac{\dot{U}_{R1\_\omega_1}}{Z_{R1\_\omega_1}} = \frac{j\omega_1 M_1 \dot{I}_{T\_\omega_1}}{Z_{R1\_\omega_1}} \tag{7}$$

So the decoupling conditions are that $U_{S1\_\omega1}$, $U_{S1\_\omega2}$, $Z_{S1\_\omega1}$, $Z_{S1\_\omega2}$ approximate to zero, and $Z_{R1\_\omega2}$ tends to infinity.

According to the above decoupling conditions and the parameter expressions in Table 3, the decoupling influence factors of receivers can be obtained, including the receivers' mutual coupling coefficient k_S, frequency separation degree k_f, and the receivers' quality factors Q_{R1} and Q_{R2}. The

TABLE 3. Parameters, definitions and expressions of the equivalent circuit.

Parameters	Definitions	Expressions
$Z_{Rm\_\omega_n}$	Loop impedance of the receiver	$Z_{Rm\_\omega_n} = r_{Rm} + R_{Rm} + j\omega_n L_{Rm} + \frac{1}{j\omega_n C_{Rm}}$
$Z_{Sm\_\omega_n}$	Reflected impedance from another receiver to this receiver	$\begin{cases} Z_{S1\_\omega_n} = \frac{\omega_n^2 M_S^2}{Z_{R2\_\omega_n}} \\ Z_{S2\_\omega_n} = \frac{\omega_n^2 M_S^2}{Z_{R1\_\omega_n}} \end{cases}$
$\dot{U}_{Rm\_\omega_n}$	Induced voltage of transmitter current	$\dot{U}_{Rm\_\omega_n} = j\omega_n M_m \dot{I}_{T\_\omega_n}$
$\dot{U}_{Sm\_\omega_n}$	Induced voltage of another receiver current	$\begin{cases} \dot{U}_{S1\_\omega_n} = j\omega_n M_S \frac{\dot{U}_{R2\_\omega_n}}{Z_{R2\_\omega_n}} \\ \dot{U}_{S2\_\omega_n} = j\omega_n M_S \frac{\dot{U}_{R1\_\omega_n}}{Z_{R1\_\omega_n}} \end{cases}$
$\dot{I}_{Rm\_\omega_n}$	Receiver current	$\dot{I}_{Rm\_\omega_n} = \frac{\dot{U}_{Rm\_\omega_n} + \dot{U}_{Sm\_\omega_n}}{Z_{Rm\_\omega_n} + Z_{Sm\_\omega_n}}$

TABLE 4. Simulated parameters and values.

Parameters	Values	Parameters	Values
f_1	20 kHz	f_2	20~100 kHz
$I_{T\_\omega_1}$	30 A	$I_{T\_\omega_2}$	10 A
L_T	100 μH	r_T	0.1 Ω
r_{R1}	0.2 Ω	r_{R2}	0.2 Ω
R_{R1}	5 Ω	R_{R2}	10 Ω
M_1, M_2	20 μH	M_S	0~50 μH
Q_{R1}	1~10	Q_{R2}	1~10
k_S	0~0.2	k_f	0~4

definitions are expressed as Equation (8) to Equation (11), respectively.

$$k_S = M_S \Big/ \sqrt{L_{R1} L_{R2}} \tag{8}$$

$$k_f = (f_2 - f_1)/f_1 \tag{9}$$

$$Q_{R1} = \omega_1 L_{R1} / (r_{R1} + R_{R1}) \tag{10}$$

$$Q_{R2} = \omega_2 L_{R2} / (r_{R2} + R_{R2}) \tag{11}$$

III. SIMULATION ANALYSIS

In order to analyze the effect of the above factors on the decoupling effect, simulations were performed. The simulated parameters and values are shown in Table 4.

A. ANALYSIS OF DECOUPLING CHARACTERISTICS

The frequency separation degree k_f can be changed by adjusting f_2. Under the conditions of different k_S, Q_{R1}, and Q_{R2}, the output power of receiver 1 P_{R1} varies with k_f, as shown in Fig. 10.

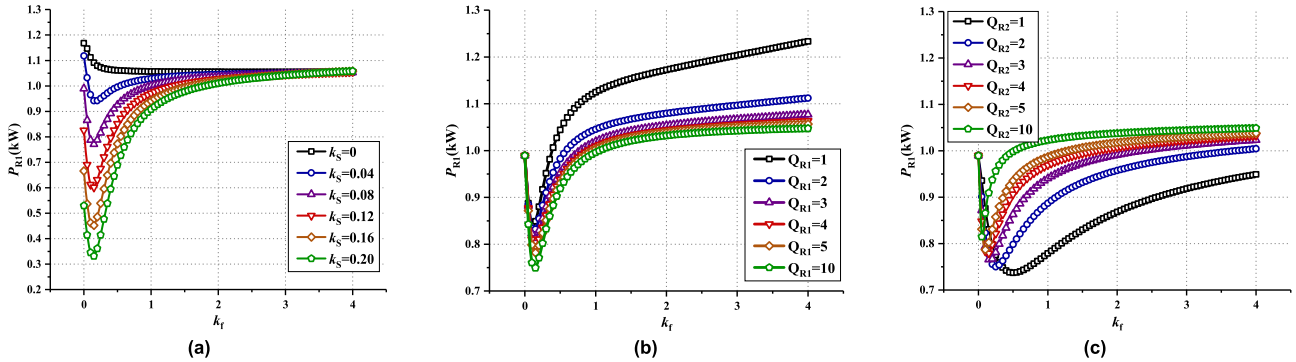

FIGURE 10. Curves of P_{R1} varying with k_f under different (a) k_S, (b) Q_{R1} and (c) Q_{R2}.

From the general trend of the curve in Fig. 10, the output power of receiver 1 decreases sharply due to mutual coupling as k_f increases, then gradually increases and finally stabilizes. Therefore, when the frequency separation degree is higher than a certain value, the output power of receiver 1 is basically not affected by the frequency of receiver 2, and power decoupling can be achieved.

In addition, according to Fig. 10, the smaller the coupling coefficient or the larger the quality factor of the two receivers, the smaller the power coupling range and the more favorable the decoupling of the dual-frequency system.

B. ANALYSIS OF EFFICACY CHARACTERISTICS

In order to analyze the efficacy characteristics of the system, f_1 and f_2 were configured as 20 kHz and 20 kHz in the single-frequency system, as 20 kHz and 85 kHz in the dual-frequency system, respectively. The corresponding frequency separation degree k_f were equal to 0 and 3.25, and the quality factors of the two receivers Q_{R1} and Q_{R2} were taken to be 6.04 and 13.08, respectively. The other parameters were consistent with Table 4.

In single-frequency and dual-frequency systems, the variation curves of output power of receiver 1 P_{R1}, output power of receiver 2 P_{R2}, total output power P_R and system efficiency η with receiver mutual coupling coefficient k_S, are shown in Fig. 11.

In the single-frequency system of Fig. 11(a), the output power of receiver 1, receiver 2, and the whole system decreases significantly as the receiver mutual coupling increases, reaching 54.7%, 19.2%, and 42.5% of the original output power, respectively. The system efficiency decreases from 91.8% to 88.3%.

In the dual-frequency system of Fig. 11(b), the output power of receiver 1, receiver 2 and the whole system does not change significantly as the receiver mutual coupling increases, varying by 3.2%, 2.5% and 1.3%, respectively. The efficiency is higher than that of the single-frequency system. It is proved that the dual-frequency system can effectively achieve power decoupling and improve the system efficiency.

In addition, in the single-frequency system, due to the mutual inductance of the receivers M_S, additional impedance Z_{TR1} and Z_{TR2} are reflected back to the transmitter, expressed

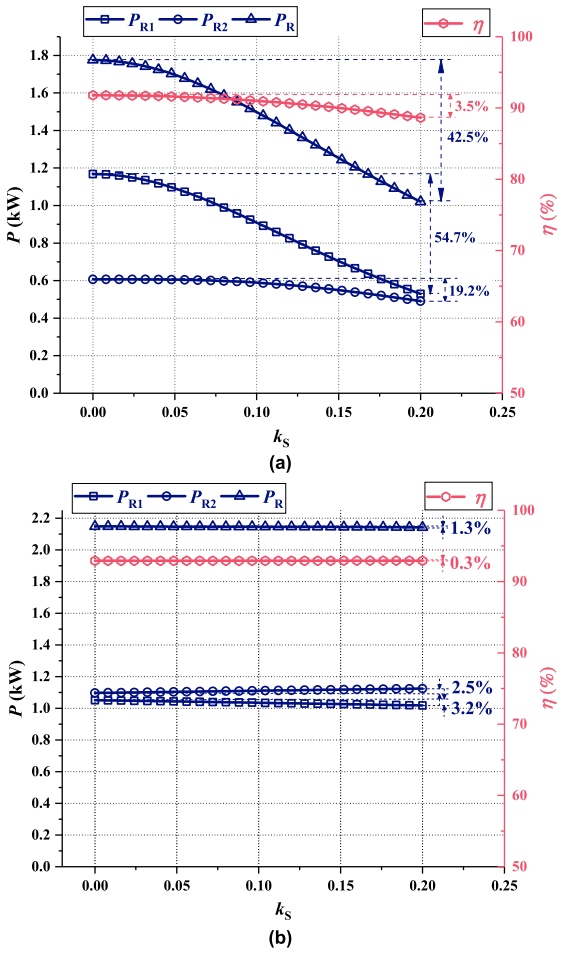

FIGURE 11. Curves of efficacy characteristics in (a) single-frequency system and (b) dual-frequency system.

as Equation (12).

$$Z_{TR1} = Z_{TR2} = -j\frac{\omega^3 M_1 M_2 M_S}{(r_{R1} + R_{R1})(r_{R2} + R_{R2})} \tag{12}$$

According to Equation (14), the reflected impedance is capacitive and proportional to M_S. It affects the resonant state of the transmitter, increases the reactive power of the inverter, and reduces its power output capability. These are the disadvantages of a single-frequency system. In a dual-frequency system, the equivalent reflected impedance is independent

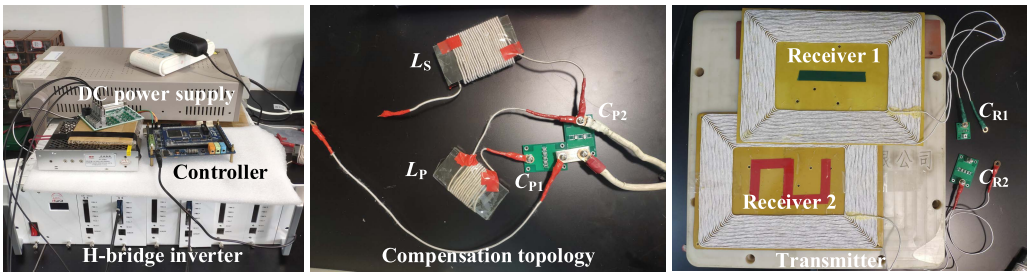

FIGURE 12. Schematic diagram of the proposed dual-frequency compatible WPT system.

TABLE 5. Parameters of the experimental platform.

Parameters	Values	Parameters	Values	Parameters	Values
E_d	0~300 V	C_{P2}	288.56 nF	C_{R1}	241.6 nF
K_A	0~1	L_T	102.84 μH	r_{R1}	261.48 mΩ
f_1	20 kHz	r_T	95.18 mΩ	R_{R1}	1 Ω
f_2	85 kHz	M_1	21.56 μH	L_{R2}	255.15 μH
L_S	102.84 μH	M_2	19.84 μH	C_{R2}	13.74 nF
L_P	25.93 μH	M_S	27.54 μH	r_{R2}	249.1 mΩ
C_{P1}	288.56 nF	L_{R1}	262.12 μH	R_{R2}	10 Ω

of each other because the output power of the two receivers is decoupled. Therefore, there is no additional reflected impedance and no drawbacks as mentioned above.

IV. PROTOTYPE AND EXPERIMENTAL VERIFICATION

An experimental platform was built to verify the proposed system, shown in Fig. 12, and its parameters are shown in Table 5. The input DC bus voltage E_d is realized by an adjustable DC power supply, and the modulation ratio K_A is adjusted in the control program.

A. VERIFICATION OF IMPEDANCE CHARACTERISTIC OF DUAL-FREQUENCY COMPENSATION TOPOLOGY

The input impedance characteristic curve of the dual-frequency compensation topology measured by the impedance analyzer in the absence of receivers is shown in Fig. 13. There are two extreme points in the curve corresponding to the two resonance points of the topology. The measured resonant frequencies are 20.016 kHz and 85.003 kHz, which are consistent with the design values.

B. VERIFICATION OF CONSTANT CURRENT CHARACTERISTICS OF DUAL-FREQUENCY COMPENSATION TOPOLOGY

In the absence of receivers, a power resistor was connected in series with the transmitter as an equivalent reflected impedance Z_{eq}. The DC bus voltage E_d and modulation ratio K_A were configured to 150 V and 0.8, respectively. At different resistor values, the transmitter current was measured and decomposed with an oscilloscope to obtain the rms values of its components at 20 kHz and 85 kHz. Curves of the transmitter current characteristics are shown in Fig. 14.

According to Fig. 14, $I_{T\_\omega 1}$ and $I_{T\_\omega 2}$ remain approximately constant when the resistance increases. It is proved

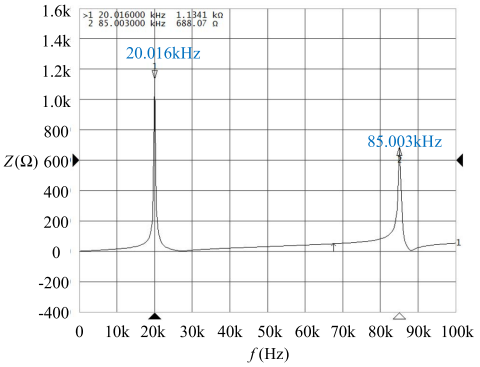

FIGURE 13. Measured input impedance characteristic curve of the dual-frequency compensation topology.

that this compensation topology has a constant current characteristic for the dual-frequency components. It should be noted that the curves decrease slightly as the resistance increases. This is because the output current of the inverter increases, the internal resistance voltage drop of the switches and resonant inductor increases, and the actual input voltage of the resonant topology decreases.

C. SYSTEM WAVEFORMS AND DECOUPLING CHARACTERISTICS VERIFICATION

The resonant frequencies of the two receivers were configured as $f_1 = 20$ kHz and $f_2 = 85$ kHz, the input voltage was configured as $E_d = 150$ V and the modulation ratio was configured as $K_A = 0.8$. The measured system waveforms are shown in Fig. 15, where channel 1 is the inverter output voltage u_{iv}, channel 3 is the transmitter current i_T, channel 2 is the output voltage of receiver 2 u_{R2} (85 kHz), and channel 4 is the output voltage of receiver 1 u_{R1} (20 kHz). The waveform of each channel was analyzed with an oscilloscope for fast Fourier transform. And the dual-frequency components of each parameter were measured as Fig. 16.

According to the experimental results in Fig. 16 (a), the inverter output voltage u_{iv} contains multiple frequency components through SPWM modulation. By dual-frequency compensation of the proposed topology, the transmitter current i_T contains two main frequency components at 20 kHz and 85 kHz, as shown in Fig. 16 (b). And its other harmonics are largely filtered out.

In Fig. 16 (c) and (d), the output voltages of the two receivers change sinusoidally. Each frequency is consistent

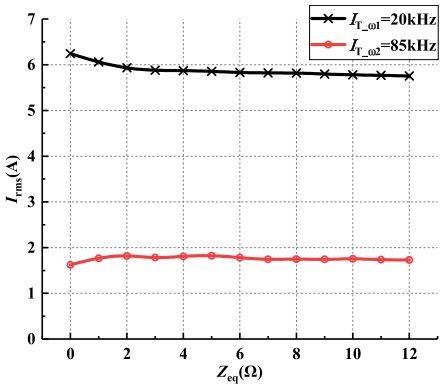

FIGURE 14. Curves of the transmitter current characteristics.

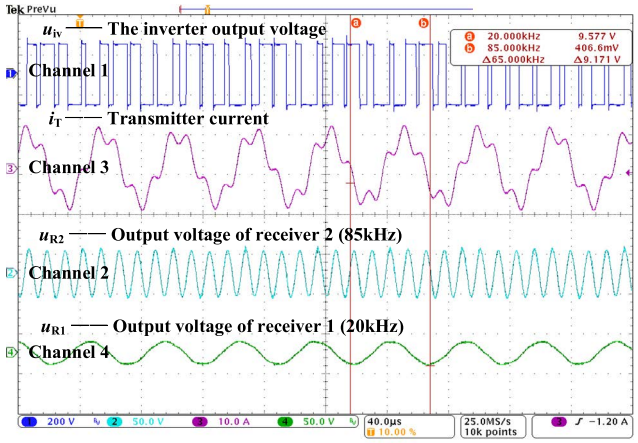

FIGURE 15. Waveforms of the dual-frequency WPT system.

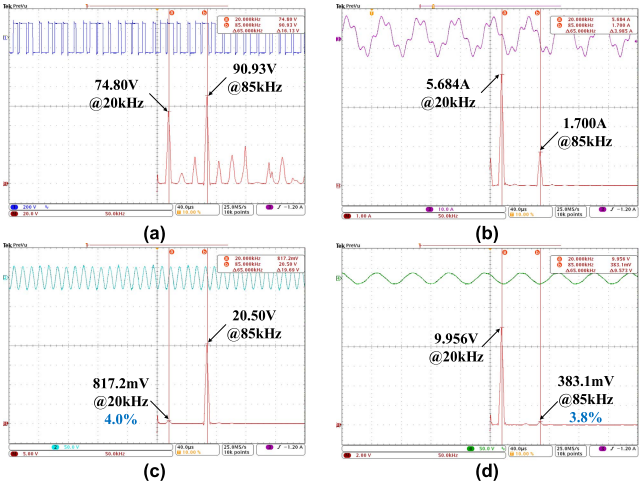

FIGURE 16. FFT results of the four channels: (a) u_{iv}(Channel 1), (b) i_T(Channel 3), (c) u_{R2}(Channel 2) and (d) u_{R1}(Channel 4).

with its natural resonant frequency, and the other frequency component has a small proportion. Therefore, through frequency-selective resonance, the decoupling of the output power has been realized.

D. VERIFICATION OF DUAL-FREQUENCY DECOUPLING MODULATION METHOD

The DC input voltage E_d adjustment range was 0 to 300 V and the modulation ratio K_A was 0 to 1. The experimental waveforms of the transmitter current were measured in the full range and their 20 kHz and 85 kHz components were obtained by Fourier decomposition. In addition, the theoretical results were calculated from Equation (5) and the simulation results were derived from the established simulation model. The transmitter current curves are shown in Fig. 17, where the red dots represent the theoretical calculation results, the black lines represent the simulation results, and the colored lines represent the experimental results. It can be seen that the experimental results are consistent with the theoretical calculation and simulation analysis.

In Fig. 17, the curves of the transmitter current varying with modulation ratio K_A and DC bus voltage E_d are obtained by taking the plane $E_d = 150$ V and $K_A = 0.8$, respectively. It can be seen that there is a monotonic relationship between the two frequency current components and a single variable.

Taking control objectives $I_{T\_\omega1} = 10$ A and $I_{T\_\omega2} = 3$ A as an example, the objective planes are produced in two diagrams and intersect the 3D surfaces at curves l_1 and l_2, respectively. the intersection of l_1 and l_2 is the value that achieves the above objective. Since the target parameters vary monotonically with the variables, the control parameters must have a set of solutions and be unique.

Therefore, by adjusting the DC bus voltage and modulation ratio, the two frequency components of the transmitter current can be adjusted independently, thus achieving power decoupling control of the receivers.

In practical applications, according to Equation (5) and Fig. 17, the adjustment range of the two transmitter current components can be flexibly configured by the input power supply and resonant cavity parameters, for meeting the output power requirements of the two receivers.

E. VERIFICATION OF THE SYSTEM'S EFFICACY CHARACTERISTICS

The output power and efficiency of the WPT system were analyzed in single-frequency and dual-frequency modes, respectively. (a) Traditional single-frequency system: the frequencies of both receiver 1 and receiver 2 were configured to 20 kHz. (b) Proposed dual-frequency system: the frequencies of receiver 1 and receiver 2 were configured to 20 kHz and 85 kHz, respectively.

Considering the regulation range of the two frequency current components, the rated operating point of the system was set to the DC input voltage $E_d = 150$ V and modulation ratio $K_A = 0.8$. The transmitter current was always 5.684 A @ 20 kHz and 1.700 A @ 85 kHz according to the constant current characteristic of the dual-frequency compensation topology. The same transmitter current was a prerequisite for comparison.

The experiments were conducted under receiver 1 only, receiver 2 only, and receiver 1 and receiver 2 conditions, respectively. The output voltages of both receivers were measured, the frequency components were obtained by Fourier decomposition, and the total output power and efficiency of

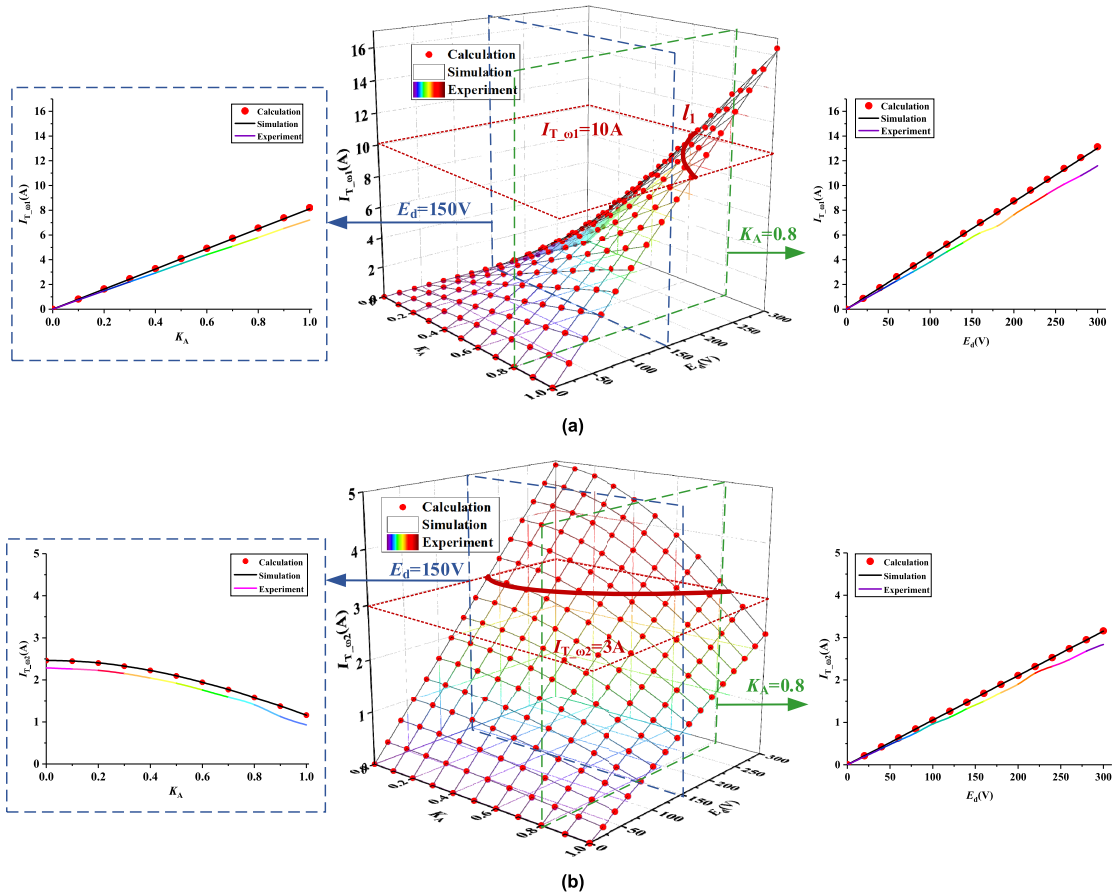

FIGURE 17. Curves of the transmitter current components varying with E_d and K_A: (a) $I_{T\_\omega1}$ and (b) $I_{T\_\omega2}$.

TABLE 6. Measured efficacy characteristics of the proposed system.

(a) Traditional single-frequency system: $f_1 = f_2 = 20$ kHz

Groups	Operating receivers	Output voltages of receiver 1	Output voltages of receiver 2	Output power of the system	Efficiencies of the system
①	Receiver 1 only	10.16 V @ 20 kHz 261.6 mV @ 85 kHz	0	103.29 W	95.9%
②	Receiver 2 only	0	24.80 V @ 20 kHz 1.599 V @ 85 kHz	61.75 W	96.2%
③	Receiver 1 and 2	7.567 V @ 20 kHz 276.6 mV @ 85 kHz	27.32 V @ 20 kHz 1.919 V @ 85 kHz	(57.34+75.00) W=132.34 W	90.0%

(b) Proposed dual-frequency system: f_1 = 20 kHz, f_2 = 85 kHz

Groups	Operating receivers	Output voltages of receiver 1	Output voltages of receiver 2	Output power of the system	Efficiencies of the system
④	Receiver 1 only	9.932 V @ 20kHz 284.4 mV @ 85kHz	0	98.73 W	96.8%
⑤	Receiver 2 only	0	356.3 mV @ 20 kHz 20.37 V @ 85 kHz	41.51 W	95.9%
⑥	Receiver 1 and 2	9.956 V @ 20kHz 383.1 mV @ 85kHz	817.2 mV @ 20 kHz 20.5 V @ 85 kHz	(99.27+40.09) W=139.36 W	95.2%

the system were calculated. Thus, six sets of experimental results were obtained from ① to ⑥ as shown in Table 6.

According to the experimental results ① ∼ ③ in Table 6, in traditional single-frequency system, the total output power changes from (103.29+61.75) W = 165.04 W working independently to 132.34W working together, a decrease of 19.8%. The system efficiency also changes from 95.9% and 96.2% to 90.0%, a decrease of 5.9%∼6.2%. Therefore, the total output power and system efficiency are significantly reduced due to the mutual coupling between receivers.

According to the experimental results ④ ∼ ⑥ in Table 6, in proposed dual-frequency system, the total output power

changes from (98.73+41.51) W = 140.24 W working independently to 139.36W working together, a decrease of only 0.6%. The system efficiency also changes from 96.8% and 95.9% to 95.2%, a decrease of only 1.6%∼0.7%. Therefore, despite the mutual coupling, the influence between the two receivers is minimal. The proposed dual-frequency system achieves the decoupling of the two coupled receivers.

According to the experimental results ③ and ⑥, the proposed dual-frequency system can improve the system efficiency by 5.2% when the total output power is basically equal.

V. CONCLUSION

In this paper, a dual-frequency compatible WPT system with a single transmitter and multiple receivers is proposed. The composition and operating principle of the system are analyzed. A dual-frequency compensation topology with two resonant frequencies is proposed, and the constant current characteristics are satisfied at each resonance point. In addition, a SPWM dual-frequency modulation method is proposed to achieve decoupling control of the two transmitter current components by adjusting the DC bus voltage and modulation ratio, so the power decoupling and independent regulation of the receivers are realized.

Simulation and experimental results show that the total output power decreases by 19.8% and the system efficiency decreases by 5.9%∼6.2% in the traditional single-frequency system due to the mutual coupling. In the dual-frequency system proposed in this paper, the total output power decreases only 0.6% and the system efficiency decreases only 1.6%∼0.7%. And on the premise of basically the same output power, the dual-frequency system improves the efficiency by 5.2%. Therefore, the proposed dual-frequency system can achieve decoupling of the receivers to avoid output power reduction and improve system efficiency.

The proposed dual-frequency system, can be used in such fields as compatibility of different frequency receivers for electric vehicle wireless charging systems, power decoupling control for multiple loads in kitchen appliances.

REFERENCES

[1] Y.-J. Kim, D. Ha, W. J. Chappell, and P. P. Irazoqui, "Selective wireless power transfer for smart power distribution in a miniature-sized multiple-receiver system," *IEEE Trans. Ind. Electron.*, vol. 63, no. 3, pp. 1853–1862, Mar. 2016.

[2] Y. Ni, J. Xu, C. Zhu, and L. Pei, "Accurate residual capacity estimation of retired $LiFePO_4$ batteries based on mechanism and data-driven model," *Appl. Energy*, vol. 305, no. 1, pp. 1–14, Jan. 2022.

[3] W. Zhong and S. Y. R. Hui, "Auxiliary circuits for power flow control in multifrequency wireless power transfer systems with multiple receivers," *IEEE Trans. Power Electron.*, vol. 30, no. 10, pp. 5902–5910, Oct. 2015.

[4] X. Gao, S. Dong, S. Cui, and C. Zhu, "Unbalanced reflected impedances and compensation of TS dynamic wireless charging system," *IEEE Trans. Ind. Electron.*, vol. 68, no. 11, pp. 10378–10387, Nov. 2021.

[5] A. Zaheer, M. Neath, H. Z. Z. Beh, and G. A. Covic, "A dynamic EV charging system for slow moving traffic applications," *IEEE Trans. Transport. Electrific.*, vol. 3, no. 2, pp. 354–369, Jun. 2017.

[6] Z. Pantic, K. Lee, and S. Lukic, "Inductive power transfer by means of multiple frequencies in the magnetic link," in *Proc. IEEE Energy Convers. Congr. Expo.*, Denver, CO, USA, Sep. 2013, pp. 2912–2919.

[7] Z. Pantic, K. Lee, and S. M. Lukic, "Multifrequency inductive power transfer," *IEEE Trans. Power Electron.*, vol. 29, no. 11, pp. 5995–6005, Nov. 2014.

[8] Z. Pantic, K. Lee, and S. M. Lukic, "Receivers for multifrequency wireless power transfer: Design for minimum interference," *IEEE Trans. Emerg. Sel. Topics Power Electron.*, vol. 3, no. 1, pp. 234–241, Mar. 2015.

[9] F. Liu, Y. Yang, Z. Ding, X. Chen, and R. M. Kennel, "Eliminating cross interference between multiple receivers to achieve targeted power distribution for a multi-frequency multi-load MCR WPT system," *IET Power Electron.*, vol. 11, no. 8, pp. 1321–1328, Jul. 2018.

[10] Z. Yan, Z. Xiang, L. Wu, and B. Wang, "Study of wireless power and information transmission technology based on the triangular current waveform," *IEEE Trans. Power Electron.*, vol. 33, no. 2, pp. 1368–1377, Feb. 2018.

[11] T. Bieler, M. Perrottet, V. Nguyen, and Y. Perriard, "Contactless power and information transmission," *IEEE Trans. Ind. Appl.*, vol. 38, no. 5, pp. 1266–1272, Sep. 2002.

[12] S. Samanta and A. K. Rathore, "Analysis and design of load-independent ZPA operation for P/S, PS/S, P/SP, and PS/SP tank networks in IPT applications," *IEEE Trans. Power Electron.*, vol. 33, no. 8, pp. 6476–6482, Aug. 2018.

[13] J. Lu, G. Zhu, D. Lin, Y. Zhang, J. Jiang, and C. C. Mi, "Unified load-independent ZPA analysis and design in CC and CV modes of higher order resonant circuits for WPT systems," *IEEE Trans. Transport. Electrific.*, vol. 5, no. 4, pp. 977–987, Dec. 2019.

XIN GAO was born in Shanxi, China. He received the B.S. and M.S. degrees from the School of Electrical Engineering and Automation, Harbin Institute of Technology, Harbin, China, in 2016 and 2018, respectively, where he is currently pursuing the Ph.D. degree.

His research interests include wireless power transfer and vehicle to grid (V2G) technology.

BOCHAO DU was born in Heilongjiang, China, in 1986. He received the B.S., M.S., and Ph.D. degrees in fault diagnosis of permanent-magnet synchronous motors from the Harbin Institute of Technology, Harbin, China, in 2009, 2011, and 2016, respectively.

He is currently with the Department of Electrical Engineering, Harbin Institute of Technology. His research interests include motor fault diagnosis and fault tolerance operation, motor parameter estimation, power electronics, and motor drivers.

YUQI ZHANG received the B.S. degree from the School of Electrical Engineering and Automation, Harbin Institute of Technology, Harbin, China, in 2020. He is currently pursuing the M.S. degree in electrical machinery and appliances.

SHUMEI CUI was born in Heilongjiang, China, in November 1964. She received the Ph.D. degree in electrical engineering from the Harbin Institute of Technology (HIT), Harbin, China, in 1998.

She has been a Professor with the Department of Electrical Engineering, HIT. Her research interests include the design and control of micro and special electric machines, electric drive system of electric vehicles, control and simulation of hybrid electric vehicles, and intelligent test and fault diagnostics of electric machines.

Dr. Cui serves as the Vice Director Member of the Micro and Special Electric Machine Committee and the Chinese Institute of Electronics and a member of the Electric Vehicle Committee and the National Automotive Standardization Technical Committee.